frontiers | Frontiers in Earth Science

TYPE Original Research
PUBLISHED 29 August 2022
DOI 10.3389/feart.2022.1000520



OPEN ACCESS

EDITED BY
Mingjun Zou,
North China University of Water Resources and Electric Power, China

REVIEWED BY
Shumin Liu,
Chongqing University, China
Peng Chen,
North China University of Science and Technology, China

*CORRESPONDENCE
Xuelong Li,
lixlcumt@126.com
Boyang Zhang,
zhangboyangzzdq@126.com

SPECIALTY SECTION
This article was submitted to Economic Geology, a section of the journal Frontiers in Earth Science

RECEIVED 22 July 2022
ACCEPTED 04 August 2022
PUBLISHED 29 August 2022

CITATION
Liu H, Zhang B, Li X, Liu C, Wang C, Wang F, Cui Z and Chen D (2022), Influence of geological structures on the occurrence of coalbed methane in Sima coal mine, China.
*Front. Earth Sci.* 10:1000520.
doi: 10.3389/feart.2022.1000520



# Influence of geological structures on the occurrence of coalbed methane in Sima coal mine, China

Hongyang Liu[1,2], Boyang Zhang[3]*, Xuelong Li[1]*, Chengwei Liu[2], Chen Wang[4], Feng Wang[1], Zhenhua Cui[3,5] and Deyou Chen[1]

[1]College of Energy and Mining Engineering, Shandong University of Science and Technology, Qingdao, China, [2]School of Mining and Mechanical Engineering, Liupanshui Normal University, Liupanshui, Guizhou, China, [3]School of Civil Engineering, Henan Polytechnic University, Jiaozuo, Henan, China, [4]School of Mining, Guizhou University, Guiyang, China, [5]Lu'an Group Sima Coal Industry Limited Company, Changzhi, Shanxi, China

Geological structures of Sima coal mine in Shanxi Province were analyzed to understand the control effect of the geological structures on the occurrence of coalbed methane (CBM) in coal seam #3 of Sima coal mine. The CBM contents in the districts #2 and #3 of Sima coal mine were tested, and the effects of buried depth, fault and collapse column on the distribution of coalbed methane content are studied. The research results showed that: 1) The average content of CBM has a linear relationship with buried depth and overburden thickness, but in the smallscale range of buried depth, the dispersion between CBM and buried depth is very large. 2) Faults and collapse columns significantly affect the content of local CBM nearby, but from the largescale range such as the whole mining area, the average value of CBM content at a certain buried depth will not be affected by faults and collapse columns. 3) In the hanging wall of F29 normal fault, it is roughly estimated that the average escape rate of CBM near the fault is 13.9%, while in the footwall of F29 normal fault, this value is 0.7%–1.1%. The results show that there is a significant difference in the influence of the fault on the CBM content in the hanging wall and footwall. 4) The control effect of collapse column on CBM occurrence is related to the development height of collapse column, the cementation degree of collapse column, groundwater runoff conditions and other factors. It can be divided into three categories: aggregation action, escape action (such as collapse column X8) and no obvious effect (such as collapse column DX7).

KEYWORDS

**occurrence of coalbed methane, geological structure, buried depth, FAULT, collapse column**

# 1 Introduction

With the rapid development and in-depth adjustment of the economy, the pattern of energy supply and demand has undergone profound changes, and the task of energy transformation and upgrading is arduous. CBM, as a clean and unconventional natural gas resource, has been generally valued by major coal-producing countries (Moore, 2012; Li et al., 2020). Moreover, CBM is one of the main disasters restricting the safe production of coal mines, and its efficient mining is a fundamental measure for mine disaster management (Zheng et al., 2019; Zhou et al., 2019; Zou Q. L. et al., 2020) and resource utilization. Meanwhile, $CH_4$, the main component of CBM, is used as a greenhouse gas (Wang et al., 2019; Li et al., 2021a). Its greenhouse effect is 21–25 times that of $CO_2$, which has a huge impact on the environment and climate. Therefore, it is vital to carry out CBM exploration and development work.

In 2020, China's underground CBM extraction production reached 14.7 billion $m^3$, accounting for 72% of the country's total CBM production (Zou et al., 2015). The geological conditions of the CBM storage areas should be clarified to ensure the efficient extraction of CBM underground. CBM is gradually formed in the long-term complex geological evolution process (Wang and Du, 2020; Zou M. J. et al., 2020; Zhou et al., 2021), so its occurrence is affected by structural evolution, depositional environment, buried depth, roof and floor lithology, coal seam thickness, hydrogeology, and magmatic activity (Xie et al., 2018; Zou et al., 2018a; Zhang C. L. et al., 2020; Kong B. et al., 2021; Zhang C. L. et al., 2021). Tectonic evolution is the key factor controlling the generation, migration, and occurrence of CBM (Zou et al., 2018b; Zhang K. Z. et al., 2020; Zhou et al., 2022).

Many scholars have studied the geological occurrence of CBM. Qin summarized the characteristics of CBM accumulation and coal reservoirs controlled by geological factors such as sedimentation, structure, coal rank, and hydrology in nine major basins in China, including Qinshui, Ordos, Junggar, Western Guizhou, Erlianhot, Hailar, etc. (Qin et al., 2018; Liu et al., 2020). Wang used mathematical statistics, literature analysis, well logging, hydrochemical analysis, and other methods to summarize the research status and development trend of the influence of hydrogeology on CBM (Wang K. et al., 2020). Ye analyzed the relationship among the structure (Pan et al., 2019), micro-pores (Liu X. F. et al., 2022), micro-cracks (Zhang et al., 2021a), and CBM content (Ma Y. K. et al., 2020; Lu et al., 2021), which is of great significance for the optimal selection of CBM production areas (Niu et al., 2019; Ye et al., 2019; Zhou et al., 2021). Sinha took a mine in India as an example to study the geological model of the CBM-enhanced recovery process (Sinha and Gupta, 2021). Fu analyzed the potential evaluation of CBM and developed sweet-spot prediction based on the developed geological conditions in the Yangjiapo block in the eastern Ordos Basin (Zou et al., 2018c). Hamilton explained the gas content trend of the Wallonia Group in the eastern part of the Surat Basin in Queensland, Australia from a geological point of view (Zhou et al., 2021). However, the existing studies rarely discuss the influence of faults and collapsed columns on the occurrence of CBM. Existing studies have shown (Zhang et al., 2005; Wang et al., 2016; Ma C. D. et al., 2020; Wang C. et al., 2020; Yu et al., 2021; Yuan et al., 2021; Liu H. Y. et al., 2022) that geological structures inevitably change the nearby ground stress field and reservoir properties (Feng et al., 2020; Feng et al., 2021; Li et al., 2021b; Shen et al., 2021; Zhang et al., 2021b), thereby affecting the occurrence of CBM (Zhang R. et al.,

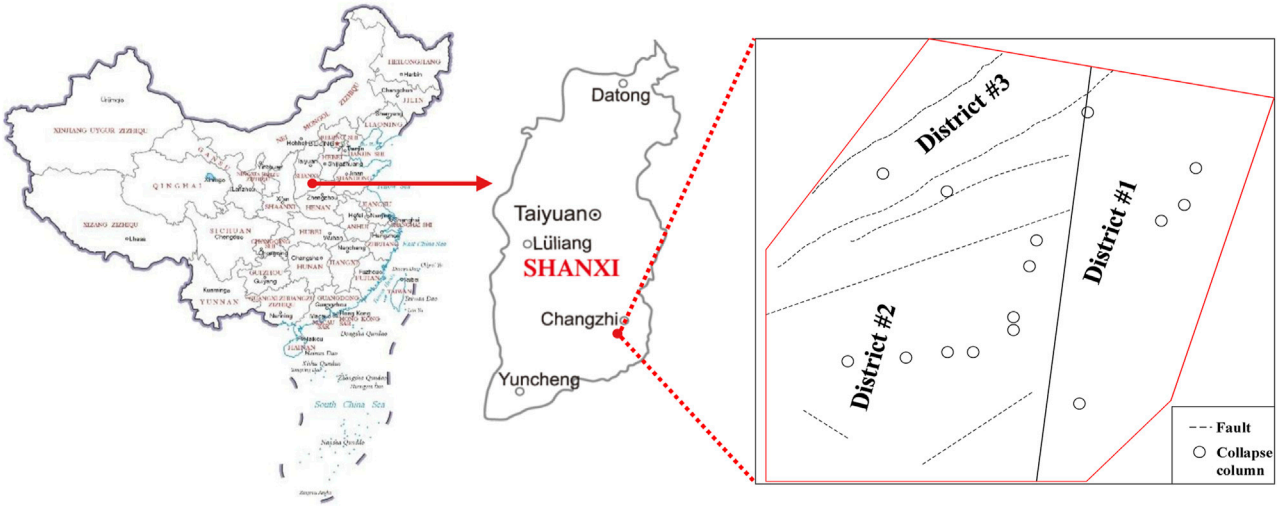


FIGURE 1
Survey of Sima coal mine.

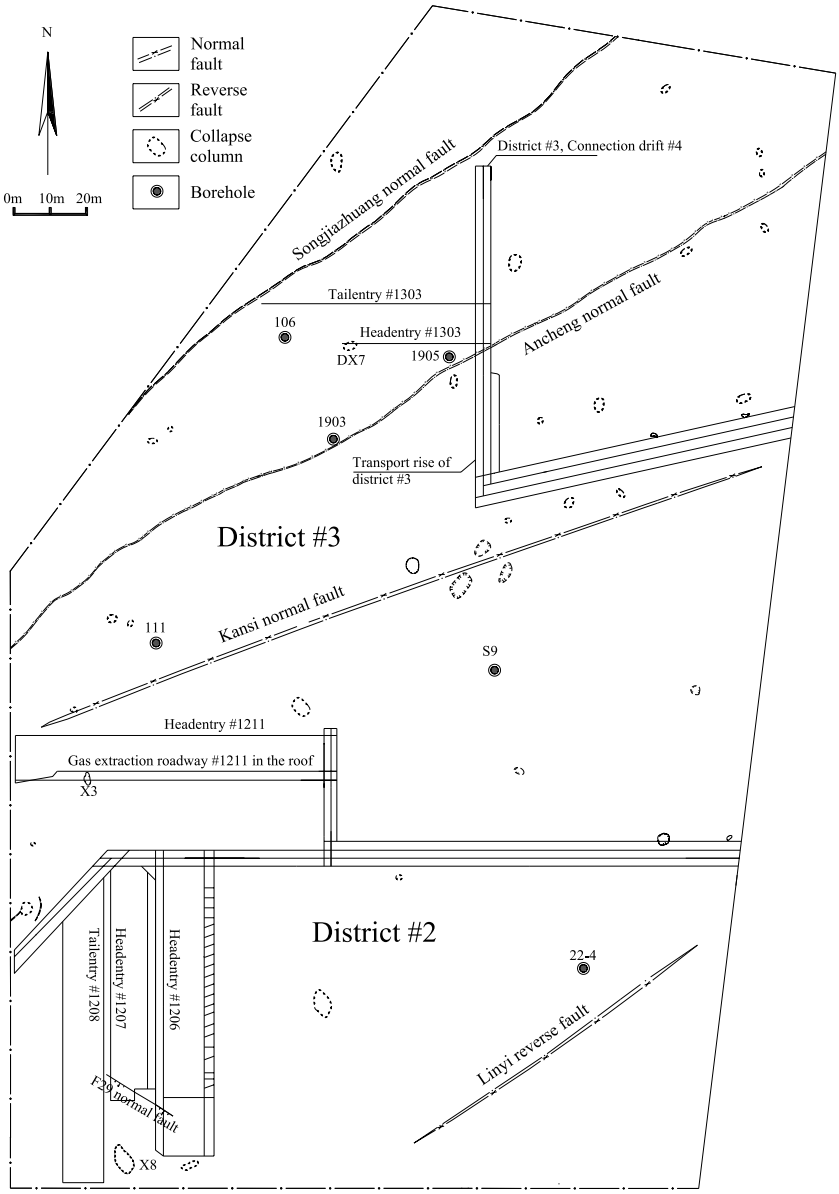


FIGURE 2
Roadway layout and main structure distribution.

2020; Kong et al., 2021a; Kong et al., 2021b). Therefore, it is necessary to study in this direction.

Shanxi Province is a major province with CBM resources in China, and the proven CBM resources are about $25.52*10^{12}$ $m^3$, accounting for 1/3 of the country's total resources (Su, 2016). The work took Sima coal mine in Changzhi County, Shanxi Province as an example to analyze the occurrence laws of CBM around geological structures such as folds, faults, and collapse columns based on the field measurement of the CBM content. On this basis, this paper studied the control effect of different geological structures on the occurrence of coalbed methane in Sima Coal Mine, especially expounded three different types of control effect and control mechanism of collapse column on the occurrence of coalbed methane, which could provid a theoretical basis for efficient underground drainage of CBM.

## 2 Geological structures of the coal mine

Sima coal mine is located in Shangdang District, Changzhi, Shanxi, China (see Figure 1), with a minefield of about

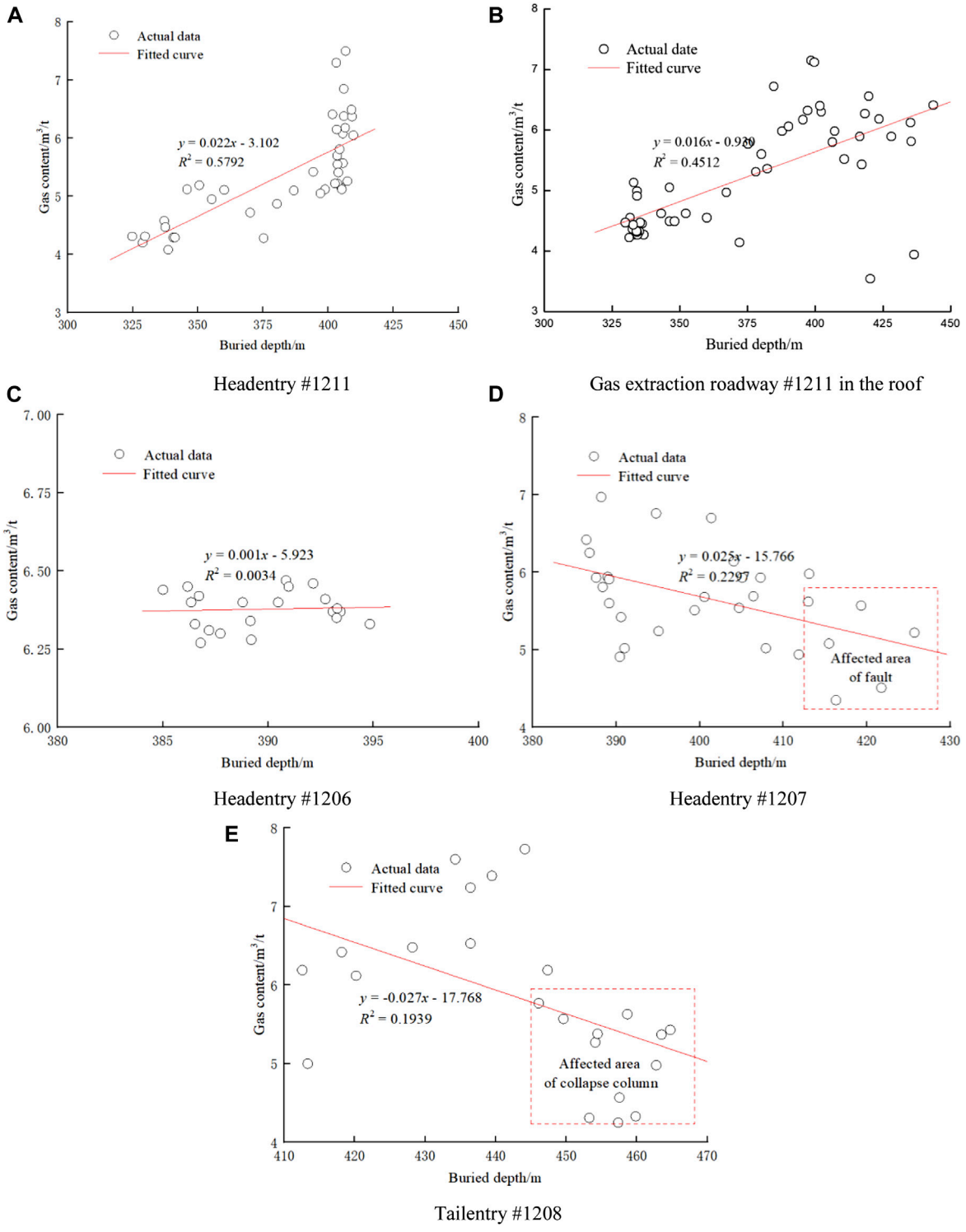


FIGURE 3
Gas content scatter with fitting curve with the increased buried depth at each panel in district #2.

TABLE 1 Linear regression relationship between the gas content and buried depth.

| Location | Linear fitting results | Correlation degree $R^2$ | Geological structure description |
|---|---|---|---|
| Headentry #1211 | $y = 0.022x - 3.101$ | 0.5791 | |
| Gas extraction roadway #1211 in the roof | $y = 0.016x - 0.930$ | 0.4512 | |
| Headentry #1206 | $y = 0.001x + 5.923$ | 0.0034 | The variation range of buried depth is small |
| Headentry #1207 | $y = 0.025x - 15.766$ | 0.2297 | There is a fault nearby |
| Tailentry #1208 | $y = 0.027x - 17.768$ | 0.1939 | There is a collapse column nearby |

29.494 km$^2$ and a recoverable reserve of 96.56 Mt. The mineable coal seams are mainly #3 and 15, and coal seam #3 is currently the main mining. The minefield is mainly divided into three districts, and the stoping of coal seam #3 in district #1 has been completed.

## 2.1 Structural-control characteristics of the mining area

Shanxi Province is located inside the ancient North China plate, which is a typical intraplate structure. The Lu'an mining area of the Sima coal mine is located in the middle section of the Zhanshang-Wuxiang-Yangcheng NNE-trending concave fold belt in the eastern part of the Qinshui block depression of the Lvliang-Taihang fault block in North China. On the west side of the fault zone, the main part is superimposed on the new rift of Changzhi. Qinshui Basin, a compound syncline coal-bearing one, is a compound syncline formed in the Yanshanian period under the background of Mesozoic compression of the North China Plate and is generally distributed in the NNE direction. The edge is surrounded by the widely exposed Paleozoic erathem, and the interior of the basin is covered by Triassic (Liu et al., 2021).

The main geological structures in the mining area is fault structure. According to its directions, it is divided into three groups of NEE-NE, NNE-SN, and NW. The first group is the most developed, with Xichuan faults, south Wenwangshan, and north faults in the north of the mining area, the south and north Ergangshan faults in the south, and Anchang and Zhonghua faults in the middle. The mining area is separated by faults, which serve as the natural boundary. The second group is followed, and the third group is mainly small faults with a drop of several meters to more than 10 m exposed by the operating mines in the east, most of which are in the NNE-SN direction. The regional tectonic pattern has gone through the stages of formation of Paleocontinental crust plate from Archean to Early Proterozoic, stable development of plate from Late Proterozoic to Early Permian, and intraplate deformation since Jurassic. The regional structure is mainly formed in the third stage—the intraplate deformation stage since the Jurassic (Cui and Jia, 2011).

## 2.2 Geological structure of the mine

The strike of the fold in the minefield can be divided into near SN and NEE directions. There are faults with different drop sizes along the strike and inclination. The strike of the fault can be divided into NW and NNE-NE directions, and most of them are tensile normal faults. The collapse columns in the minefield are relatively developed, and 15 collapse columns are directly exposed, concentrated in district #2. Figure 2 shows the layout of roadways in districts and the distribution of main geological structures in the mine.

# 3 Influence of structures on the occurrence of CBM

## 3.1 Influence of buried depths on the occurrence of CBM

At present, the stoping of the coal seam #3 in district #1 of Sima coal mine is completed. Meanwhile, the CBM content in district #1 is generally low, and it is of no practical significance to discuss the occurrence of CBM in district #1. Therefore, the influence of the geological structure of the districts #2 and #3 of Sima Coal Mine on the occurrence of CBM is studied.

### 3.1.1 District #2

The layout of the panel in the district #2 has been completed, and the CBM test points are mainly distributed at panels #1206, 1207, 1208, and 1211. Figure 3 shows the scatters with fitting curves of the CBM contents at panels #1206, 1207, 1208, and 1211 with the increased buried depths. Figures 3A,B illustrate that in the headentry and gas extraction roadway in the roof of panel #1211, the CBM content increases with the increased buried depth. The variation range of the buried depths of the headentry of panel #1206 is only about 10 m, which is far less than the variation range of the buried depths above 100 m of the panel #1211. Within a relatively small variation range of burial depth, the CBM content is highly dispersed with the burial depth, showing a slight increase trend as a whole, as shown in Figure 3C. In Figures 3D,E, the CBM contents of the headentry #1207 and

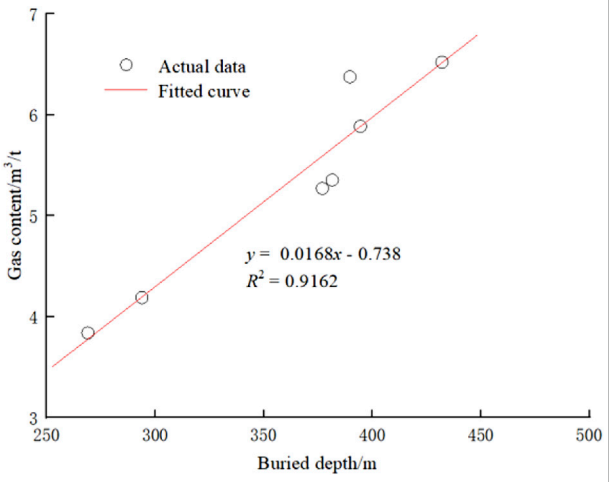


FIGURE 4
Gas content scatter with fitting curve with the increased buried depth in district #2.

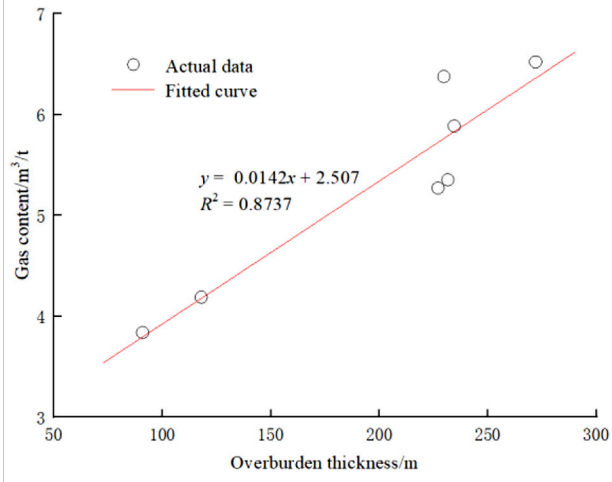


FIGURE 5
Gas content scatter with fitting curve with the overburden thickness in district #2.

tailentry #1208 decrease with the increased buried depth, what is inconsistent with conventional understanding. This result is due to the existence of F29 fault and collapse column near the headentry #1207 and tailentry #1208 respectively (Figure 2), and the CBM content is affected by the fault and collapse column. At the same time, it also shows that the influence of fault and collapse column on CBM content is significantly greater than that of buried depth.

For a unified explanation, the regression analysis method is used to establish the regression relationship between the CBM content and the buried depth of the coal seam. The linear relationship between the CBM content ($y$) and coal seam depth 10) is obtained to establish the following mathematical model.

Regression equation:

$$y = ax + b$$

where $y$ represents the CBM content; $x$ represents the buried depth of the coal seam; $a$ and $b$ represent the undetermined coefficients.

Table 1 shows the linear regression relationship between the CBM content and buried depth at panels #1206, 1207, 1208, and 1211.

Due to the influence of the small variation range of buried depth or the influence of faults and collapse columns, the CBM content of panel #1206, #1207 and #1208 have no significant linear relationship with buried depth. However, combined with the test data of CBM observation holes #9 and #22–4 in the district #2, we calculated the average value of CBM content at each measurement point, and plotted the variation curve of the average content of CBM with the increase of buried depth (Figure 4).

Figure 4 shows that the average CBM content increases with the increase of buried depth. The correlation degree ($R^2$) of the linear fitting is 0.9162, which is much greater than the linear fitting correlation of the test results of each panel. This shows that: 1) In the small-scale range of buried depth, the dispersion between CBM and buried depth is very large. It is meaningless to discuss the relationship between CBM content and buried depth. 2) Faults and collapse columns significantly affect the content of local CBM nearby, but from the large-scale range such as the whole mining area, the average value of CBM content at a certain buried depth will not be affected by faults and collapse columns.

In the linear relationship in Figure 4, b = −0.738, that is, when the buried depth is 0, the CBM content is negative, which has no practical significance. When calculating the buried depth of a measuring point, we used the same elevation of the ground to calculate the difference value, which is not rigorous enough. Considering the change of terrain and replacing the buried depth of a measuring point with the thickness of overburden, we get the variation relationship between the average content of CBM and the thickness of overburden, and the linear fitting parameter b becomes 2.507, as shown in Figure 5. Therefore, it is of more practical significance to discuss the relationship between CBM content and overburden thickness.

### 3.1.2 District #3

At present, only the main roadway and the headentry and tailentry of panel #1303 have been excavated in district #3 of Sima coal mine. Table 2 shows the basic parameters of CBM in the tailentry of panel #1303, and the maximum CBM content is about 4.5 $m^3$/t. The test results of CBM content of panel #1303, boreholes #111, #106, #1903, #1905, connecting entry #4 and belt roadways in the District #3 are comprehensively analyzed, and the variation curve of average CBM content with the increase of buried depth is drawn

TABLE 2 Test results of basic parameters of CBM in tailentry #1303.

| Distance between measuring position and roadway exit/m | CBM content of raw coal/($m^3$/t) | Distance between measuring position and roadway exit/m | CBM content of raw coal/($m^3$/t) |
|---|---|---|---|
| 5.6 | 4.3901 | 584.4 | 4.1096 |
| 49.3 | 4.4087 | 633.3 | 3.9290 |
| 97.9 | 4.4779 | 682.4 | 3.7528 |
| 142.4 | 4.3374 | 731.1 | 3.7647 |
| 192.3 | 4.4002 | 779.6 | 3.8316 |
| 241.6 | 4.2651 | 828.6 | 3.7937 |
| 290.4 | 4.0892 | 877.3 | 3.8076 |
| 339.6 | 4.1124 | 926.7 | 3.8311 |
| 388.3 | 3.9184 | 975.3 | 3.9661 |
| 437.8 | 4.1154 | 1024.0 | 4.223 |
| 486.4 | 4.2138 | 1072.9 | 4.4407 |
| 535.6 | 4.1257 | | |

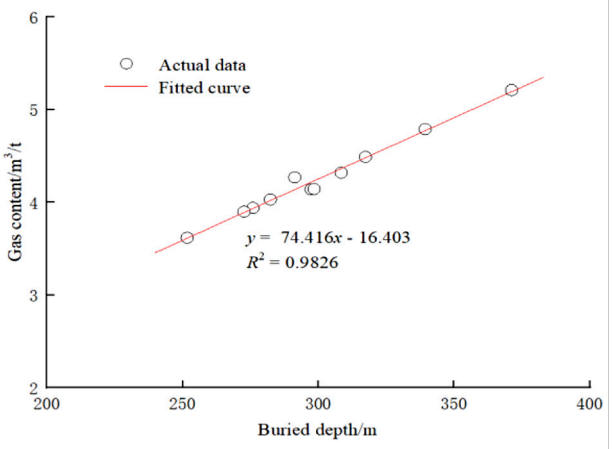


FIGURE 6
Gas content scatter with fitting curve with the increased buried depth in district #3.

(Figure 6). The fitting results are good, and the correlation coefficient reaches 0.9826. This further shows that the average value of CBM content is highly linear with the buried depth.

## 3.2 Influence of faults on the occurrence of CBM

Faults destroy the continuity and integrity of coal seams. The influence of faults on the occurrence of CBM mainly depends on its openness or sealing. The fault strike of Sima Coal Mine can be divided into NW direction and NNE-NE direction. Most of them are tensile faults with good permeability, which is conducive to the emission of CBM (Figure 7). This is because pores and fissures are widely developed in tectonic rock and two-wall rock in the fault zone of tensional or tensional shear normal fault, which provides a good channel for gas escape. On the one hand, it reduces the risk of CBM outbursts during coal mining. On the other hand, it is not conducive to the formation of CBM resources in Sima coal mine, which is difficult for the centralized mining of CBM.

Kansi normal fault and F29 normal fault were taken as examples to illustrate the control effect of Sima coal mine fault on CBM.

### 3.2.1 Kansi normal fault

The largest fault in the Sima coal mine is the Kansi normal fault, which is also the boundary between districts #2 and #3. Figure 8 shows the CBM content and seamfloor elevation in some areas around the Kansi normal fault. Obvious differences exist in the CBM content on both sides of the Kansi normal fault at the same elevation. At the same coal seam-floor elevation of 580 m, the CBM content of district #3 on the north side of Kansi fault is between 6.1–6.4 $m^3$/t, while that of district #2 on the south side of Kansi fault is 5.5–5.8 $m^3$/t. At the same elevation, there are obvious differences in the CBM content between the north and south sides of Kansi fault, indicating that Kansi fault is a barrier to migrating CBM.

### 3.2.2 F29 normal fault

F29 normal fault is located in panel #1207, and the outer edges of both sides reach panels #1208 and #1206. The fall of F29 normal fault is 3.3 m. Compared with Kansi fault, the scale and fall of F29 normal fault are much smaller, but there are still significant differences in gas content between hanging wall and footwall of the fault, as shown in Figure 9. This further shows that

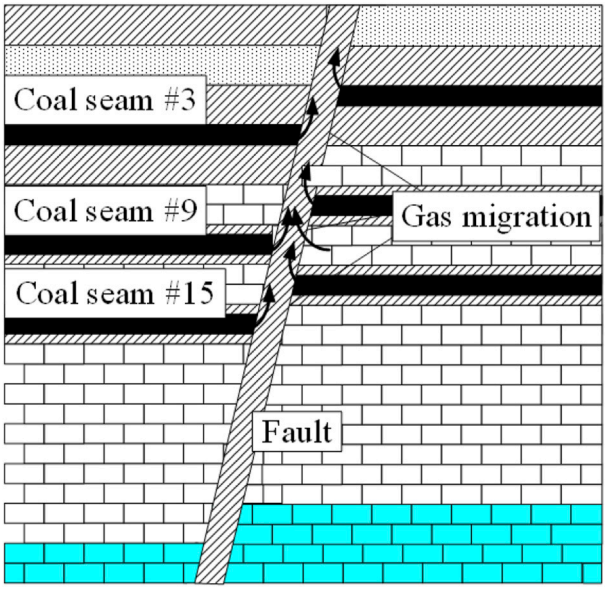


FIGURE 7
Control effect of faults in Sima coal mine on CBM.

no matter the size of the fault, it can obstruct the occurrence of CBM.

The CBM content at the headentry and setup entry of panel #1207 on the hanging wall of F29 normal fault is between 4.35 and 5.57 $m^3/t$, with an average value of 4.96 $m^3/t$. The corresponding buried depth of the measuring points is 411–425 m, with an average of 417.8 m. From the previous analysis, we know that although the fault can affect the occurrence of CBM in a certain range nearby, it will not change the average CBM content in a certain buried depth in a large-scale range. The buried depth of the headentry and setup entry of panel #1207 changes little as a whole. The average CBM content of all measuring points in the headentry and setup entry of panel #1207 is 5.64 $m^3/t$. Based on this, we can roughly estimate that the escape rate of CBM in the hanging wall of F29 normal fault is (5.64–4.96)/4.96 = 13.9%.

The CBM content of each measuring point in the headentry and setup entry of panel #1207 on the hanging wall of F29 normal fault is less than the overall average of the CBM content of the two roadways. The distance between these measuring points and F29 normal fault is 8.9–98.6 m (Figure 9). It shows that the influence radius of CBM escape in the hanging wall of F29 normal fault should be more than 100 m.

The CBM content of all measuring points in tailentry of panel #1207 at the foot-wall of F29 normal fault is 6.33–6.47 $m^3/t$, with an average of 6.40 $m^3/t$. The buried depth of all measuring points is 385–394m, with an average of 389.5 m. The CBM content of the three measuring points closest to F29 normal fault is 6.33–6.35 $m^3/t$, with an average of 6.34 $m^3/t$, and the buried depth is 389–394 m, with an average of 392 m. Compared with the overall average CBM content, the CBM content at these three points decreased by 0.7, 1.1, and 0.9% respectively.

The above results show that there is a significant difference in the influence of the fault on the CBM content in the hanging wall

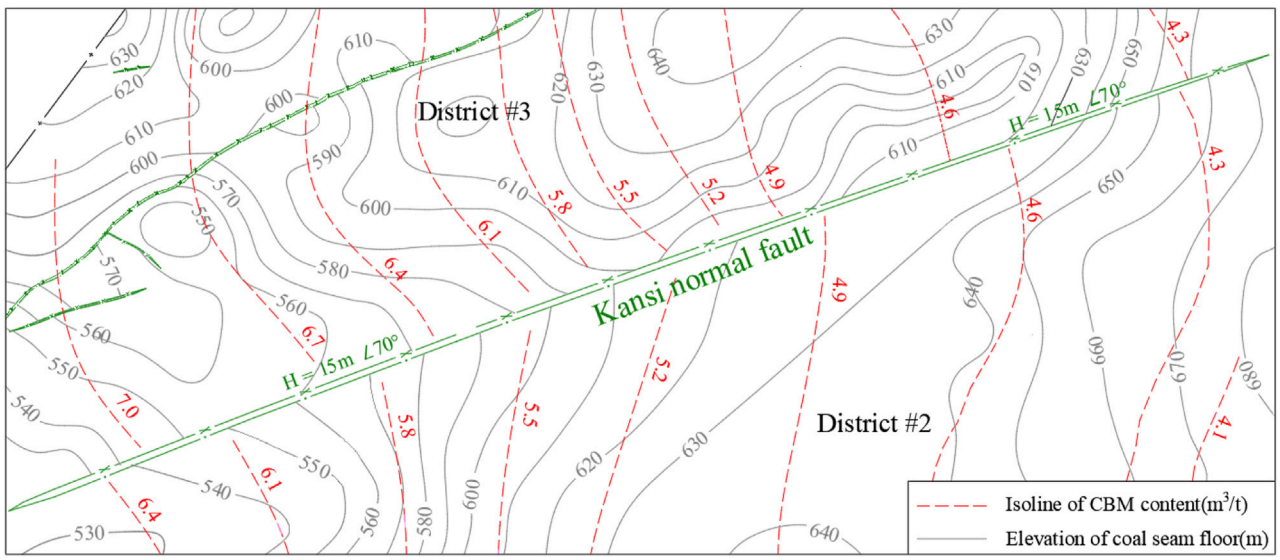


FIGURE 8
Gas content and elevation of the coal seam floor around Kansi fault.

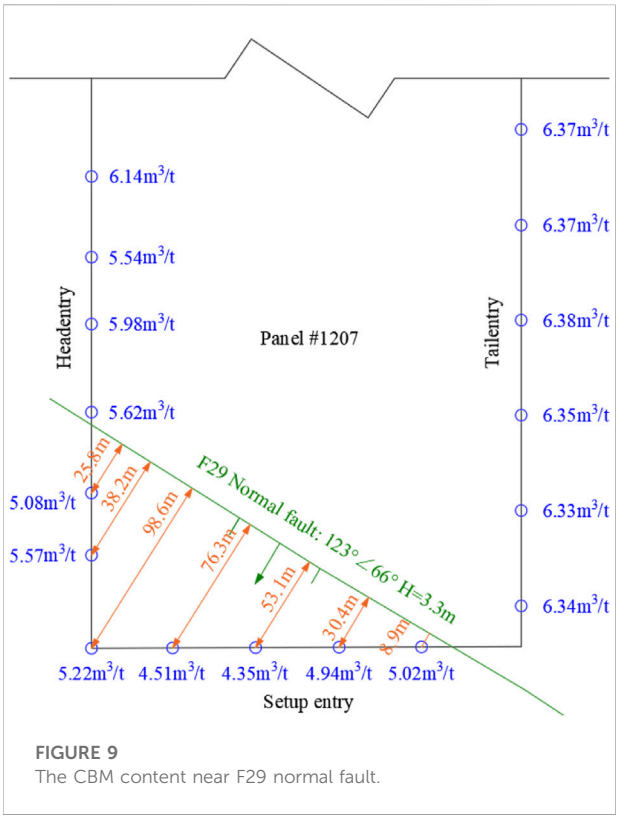


FIGURE 9
The CBM content near F29 normal fault.

and footwall, which needs to be analyzed in combination with the lithology, structural stress and other factors of the two walls.

## 3.3 Influence law of collapse columns on the occurrence of CBM

### 3.3.1 Types of controlling effect of collapse column on CBM occurrence

Collapse column is the collapse phenomenon of soluble rocks such as limestone and dolomite in the lower part of coal measure stratum under the action of groundwater and gravity. In the process of studying the formation mechanism of collapse columns, experts and scholars have formed theories such as "karst cave theory", "paste dissolution theory" and "vacuum suction collapse theory". Although there is no unified theory at present, it is generally believed that the development of collapse columns is controlled by three factors: karst conditions, hydrodynamic conditions and tectonic action. Sima Coal Mine has sufficient hydrodynamic conditions, fully developed karst, well-developed structural conditions in the process of geological evolution, and has the basic conditions for the development of collapse columns, resulting in the distribution of collapse columns in all areas of Sima Coal Mine.

The controlling effect of collapse column on CBM occurrence is related to the development height of collapse column, the cementation degree of collapse column, groundwater runoff conditions and the positional relationship between collapse column and other fault structures, which can be mainly divided into the following three categories:

#### 3.3.1.1 Aggregation action

The minable coal seams in Sima coal mine are mainly 3 layers, coal seams #3, #9 and #15. The top of the collapse column may develop to the roof of coal seam #3 or only to the floor of coal seam #3. If the top of the collapse column develops to the roof of coal seam #3, the internal cementation is very poor and is not connected with other fault structures, the collapse column will become the vertical migration channel of coalbed methane. In general, the CBM content in deep coal seams is high and the pressure is high. The CBM existing in coal seams #9 and #15 migrate to coal seam #3 along the collapse column, and the CBM accumulation area is formed around the collapse column (Figure 10A).

#### 3.3.1.2 Escape action

When the collapse column penetrates coal seams #3, #9 and #15, if the water barrier capacity inside the collapse column is very poor, Ordovician limestone water or water from the roof and floor of the coal seam may enter the working face through the collapse column, resulting in increased water inflow of the working face and even mine water damage. At this time, under the pressure of water, the CBM in the rock gap gradually precipitates and the CBM escapes (Figure 10B). At the same time, the flow of water will dissolve a small part of the CBM on the one hand and accelerate the CBM escape on the other hand. In addition, if the collapse column is connected with other fault structures to form a CBM drainage channel, the CBM content will also be reduced and the CBM will escape.

#### 3.3.1.3 No obvious effect

When the collapse column does not penetrate into the floor of coal seam #3, and there is a thick and complete rock stratum with poor permeability between the floor of coal seam #3 and the collapse column, the existence of the collapse column will not have a significant impact on the CBM content of the coal seam #3 (Figure 10C). In addition, if the internal cementation of the collapse column is good and the mechanical and seepage indexes of the complete rock sample have been basically reached, and the top of the collapse column develops to the roof of the coal seam #3 in time, the existence of the collapse column will also not cause significant changes in the CBM content of the coal seam #3.

### 3.3.2 Collapse column X8

Collapse column X8 is located on the east side of tailentry #1208 (Figure 11), and the minimum distance from the tailentry is about

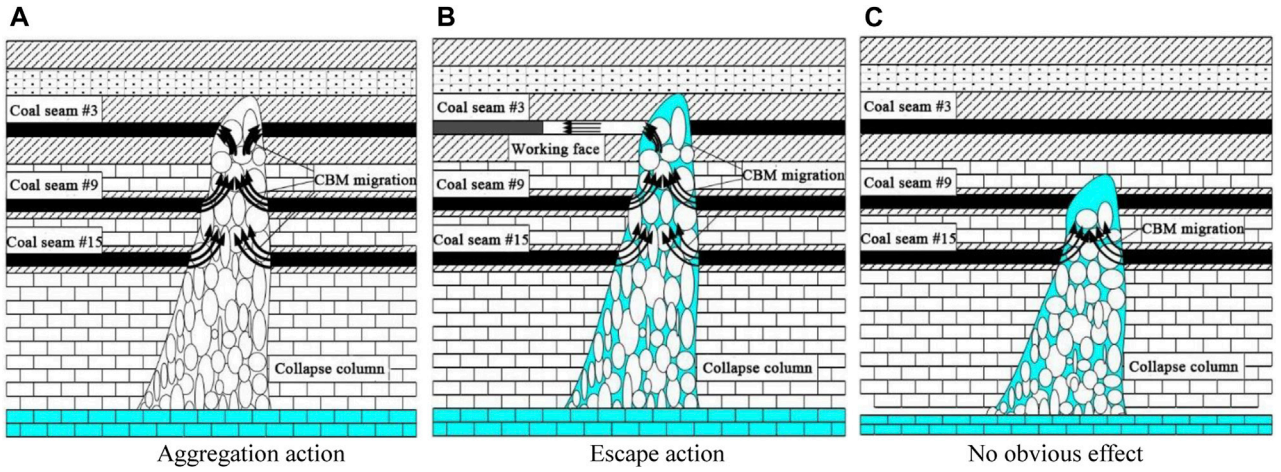


FIGURE 10
Different control effects of collapse column on the occurrence of CBM.

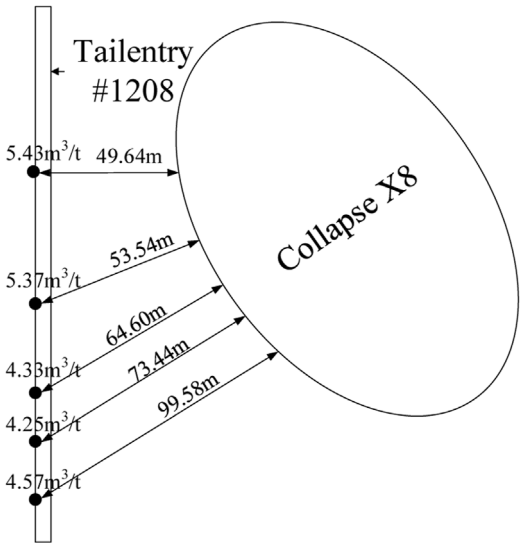


FIGURE 11
Gas occurrence rule around collapse column X8.

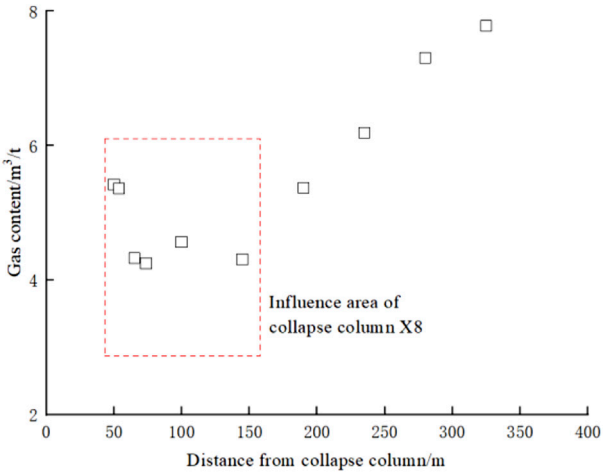


FIGURE 12
Influence radius of collapse column X8.

50 m, with the diameter of its major axis of 150 m and that of its minor axis of 50–60 m. Panel #1208 does not directly expose collapse column X8, and the drilling results show that collapse column X8 is more likely to exist.

The CBM measurement points around collapse column X8 are mainly located in tailentry #1208. If the calculation is carried out according to the linear relationship between the fitted CBM content and the buried depth in Figure 4, the gas content in the area where collapse column X8 is located should reach more than 6.50 $m^3$/t under the action of buried depth only. According to this calculation, the content of CBM near the collapse column X8 decreased by 16.4%–34.6%, with an average of 26.3%. This shows that collapse column X8 plays a major role in the escape of CBM.

Figure 12 shows that the CBM content within 150 m around collapse column X8 decreases significantly, and the minimum CBM content reaches 4.25 $m^3$/t. In the range of 150–300 m, the CBM content shows a gradual increase, and when the distance reaches about 300m, the CBM content reaches more than 6.50 $m^3$/t. So, It can be judged that the significant influence

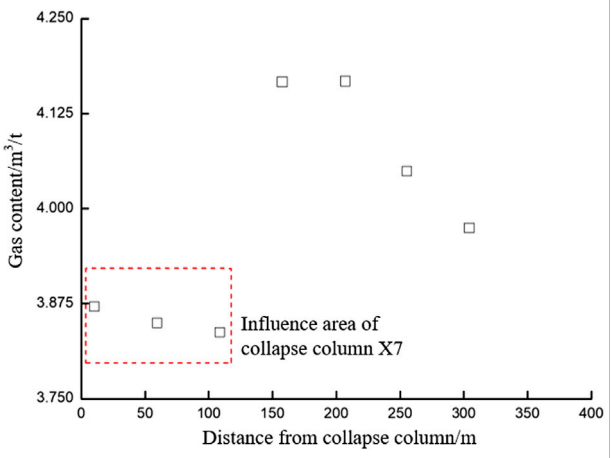


FIGURE 13
Influence radius of collapse column DX7.

radius of collapse column X8 is about 150 m, and the maximum influence radius may reach 300 m. The fractures in the formation process of collapse column provide a channel for coalbed methane transportation. The larger the fracture range is, the larger the gas escape range is.

### 3.3.3 Collapse column DX7

Collapse column DX7 is located at 595–650 m in headentry #1303 of Sima coal mine, with a major-axis diameter of about 70 m and a minor-axis diameter of about 40 m. Headentry of panel #1303 directly exposes and diagonally passes through collapse column DX7. Since panel # 1303 is the first working face in district #3, the CBM measurement points around collapse column DX7 are mainly distributed in headentry #1303.

It can be seen from Figure 13 and Table 3 that the CBM content around collapse column DX7 is not significantly reduced, and the CBM content within 50 m around collapse column DX7 is only reduced by about 7%. On the one hand, the scale of collapse column DX7 is small, and the cracks around it are not developed, which is not conducive to CBM escape; On the other hand, according to the field observation, the collapse column DX7 is well consolidated, and some areas are cemented and diagenesis again, which can not provide a good channel for CBM escape. Therefore, the CBM dissipation effect of collapse column DX7 is not obvious, and the maximum influence radius of CBM dissipation is only about 50 m.

## 4 Conclusion

Based on the actual measurement results of the occurrence of CBM in districts #2 and #3 of Sima coal mine, the effects of buried depth, fault and collapse column on CBM occurrence are analyzed. The control effect of different structures on the occurrence of CBM can provide a theoretical basis for efficient underground CBM drainage. The main conclusions are as follows:

1) The variation law of CBM content with buried depth is analyzed. The results show that: (1) In the small-scale range of buried depth, the dispersion between CBM and buried depth is very large. It is meaningless to discuss the relationship between CBM content and buried depth. (2) Faults and collapse columns significantly affect the content of local CBM nearby, but from the large-scale range such as the whole mining area, the average value of CBM content at a certain buried depth will not be affected by faults and collapse columns. (3) The average content of CBM has a linear relationship with buried depth and overburden thickness, and it is more practical to analyze the influence of overburden thickness on the average content of CBM.
2) In the hanging wall of F29 normal fault, it is roughly estimated that the average escape rate of CBM near the fault is 13.9%, while in the footwall of F29 normal fault, this value is 0.7%–1.1%. The results show that there is a significant difference in the influence of the fault on the CBM content in the hanging wall and footwall, which needs to be

TABLE 3 Test results of basic parameters in headentry #1303.

| Distance between measuring position and roadway exit/m | CBM content of raw coal/($m^3$/t) | Distance between measuring position and roadway exit/m | CBM content of raw coal/($m^3$/t) |
|---|---|---|---|
| 8.6 | 4.7543 | 289.6 | 3.9742 |
| 23.4 | 4.9372 | 338.6 | 4.0488 |
| 34.6 | 4.3518 | 387.1 | 4.1672 |
| 49.2 | 4.3657 | 436.4 | 4.1663 |
| 95.4 | 4.2045 | 485.3 | 3.8370 |
| 144.3 | 4.0503 | 534.7 | 3.8493 |
| 192.9 | 4.0206 | 583.9 | 3.8712 |
| 242.0 | 3.9648 | 632.6 | 3.7401 |

analyzed in combination with the lithology, structural stress and other factors of the two walls.

3) The control effect of collapse column on CBM occurrence is related to the development height of collapse column, the cementation degree of collapse column, groundwater runoff conditions and other factors. It can be divided into three categories: aggregation action, escape action (such as collapse column X8) and no obvious effect (such as collapse column DX7).

## Data availability statement

The original contributions presented in the study are included in the article/supplementary material, further inquiries can be directed to the corresponding authors.

## Author contributions

HL data curation and formal analysis, BZ and XL funding acquisition and investigation, CL, CW, and FW methodology, project administration and resources ZC and DC software, supervision and validation.

## Funding

This work was supported by the National Natural Science Foundation of China (52104204, 51778215, 52174072), the Education Department of Guizhou Province Fund (Qianjiaohe KY Zi [2017] 265, Qianjiaohe KY Zi [2017] 266, Qianjiaohe KY Zi [2019] 073, Qianjiaohe KY Zi [2020] 050, Qianjiao XKTJ [2020] 23), the Science and Technology Department of Guizhou Province Fund [Qiankehe Platform Talent (2019) 5620, Qiankehe Platform Talent-YSZ (2021) 001], the Natural Science Foundation of Shandong Province (ZR2021QE170), the Liupanshui Science and Technology Bureau fund (52020-2018-04-08).

## Acknowledgments

We would like to thank the Lu'an Group Sima Coal Industry Limited Company for providing part of research data for this study.

## Conflict of interest

Author ZC was employed by Lu'an Group Sima Coal Industry Limited Company

The remaining authors declare that the research was conducted in the absence of any commercial or financial relationships that could be construed as a potential conflict of interest.

## Publisher's note



## References

Cui, H. Q., and Jia, B. S. (2011). The research on gas geology rule and gas outburst danger zone prediction at sima coal mine. *J. Henan Polytech. Univ. Nat. Sci.* . 30 (2), 131–136. (in Chinese with English abstract). doi:10.16186/j.cnki.1673-9787.2011.02.022

Feng, J. J., Wang, E. Y., Huang, Q. S., Ding, H. C., and Ma, Y. K. (2020). Study on coal fractography under dynamic impact loading based on multifractal method. *Fractals* 28 (1), 2050006. doi:10.1142/S0218348X20500061

Feng, F., Chen, S. J., Wang, Y. J., Huang, W. P., and Han, Z. Y. (2021). Cracking mechanism and strength criteria evaluation of granite affected by intermediate principal stresses subjected to unloading stress state. *Int. J. Rock Mech. Min. Sci. (1997).* 143 (7), 104783. doi:10.1016/j.ijrmms.2021.104783

Kong, B., Liu, Z., and Yao, Q. G. (2021). Study on the electromagnetic spectrum characteristics of underground coal fire hazardous and the detection criteria of high temperature anomaly area. *Environ. Earth Sci.* 80 (3), 89–11. doi:10.1007/s12665-021-09380-5

Kong, X. G., Li, S. G., Wang, E. Y., Ji, P. F., Wang, X., Shuang, H. Q., et al. (2021a). Dynamics behaviour of gas-bearing coal subjected to SHPB tests. *Compos. Struct.* 256, 113088. doi:10.1016/j.compstruct.2020.113088

Kong, X. G., Li, S. G., Wang, E. Y., Wang, X., Zhou, Y. X., Ji, P. F., et al. (2021b). Experimental and numerical investigations on dynamic mechanical responses and failure process of gas-bearing coal under impact load. *Soil Dyn. Earthq. Eng.* 142, 106579. doi:10.1016/j.soildyn.2021.106579

Li, X. L., Cao, Z. Y., and Xu, Y. L. (2020). Characteristics and trends of coal mine safety development. *Energy Sources Part A Recovery Util. Environ. Eff.* 2020, 1–19. doi:10.1080/15567036.2020.1852339

Li, X. L., Chen, S. J., Liu, S. M., and Li, Z. H. (2021a). AE waveform characteristics of rock mass under uniaxial loading based on Hilbert-Huang transform. *J. Cent. South Univ.* 28 (6), 1843–1856. doi:10.1007/s11771-021-4734-6

Li, X. L., Chen, S. J., Wang, S., Zhao, M., and Liu, H. (2021b). Study on *in situ* stress distribution law of the deep mine taking Linyi mining area as an example. *Adv. Mater. Sci. Eng.* 2021, 5594181–5594211. doi:10.1155/2021/5594181

Liu, S. M., Li, X. L., Wang, D. K., and Zhang, D. M. (2020). Investigations on the mechanism of the microstructural evolution of different coal ranks under liquid nitrogen cold soaking. *Energy Sources Part A Recovery Util. Environ. Eff.* 2020, 1–17. doi:10.1080/15567036.2020.1841856

Liu, X. F., Nie, B. S., Guo, K. Y., Zhang, C. P., Wang, Z. P., and Wang, L. K. (2021). Permeability enhancement and porosity change of coal by liquid carbon dioxide phase change fracturing. *Eng. Geol.* 287, 106106. doi:10.1016/j.enggeo.2021.106106

Liu, H. Y., Zhang, B. Y., Li, X. L., Liu, C. W., Wang, C., Wang, F., et al. (2022). Research on roof damage mechanism and control technology of gob-side entry retaining under close distance gob. *Eng. Fail. Anal.* 138, 106331. doi:10.1016/j.engfailanal.2022.106331

Liu, X. F., Wang, L. K., Kong, X. G., Ma, Z. T., Nie, B. S., Song, D. Z., et al. (2022). Role of pore irregularity in methane desorption capacity of coking coal. *Fuel* 314, 123037. doi:10.1016/j.fuel.2021.123037

Lu, J. X., Li, H., Shi, S. L., Huang, B. X., Lu, Y., Li, M., et al. (2021). Microwave-induced microstructure evolution of coal and its effects on the methane adsorption characteristic. *Energy fuels.* 35 (5), 4081–4090. doi:10.1021/acs.energyfuels.0c04363

Ma, C. D., Li, X. B., Chen, J. Z., Zhou, Y. N., and Gao, S. (2020). Geological core ground reorientation technology application on *in situ* stress measurement of an over-kilometer-deep shaft. *Adv. Civ. Eng.* 2020, 1–13. doi:10.1155/2020/8830593

Ma, Y. K., Nie, B. S., He, X. Q., Li, X. C., Meng, J. Q., and Song, D. Z. (2020). Mechanism investigation on coal and gas outburst: An overview. *Int. J. Min. Metall. Mater.* 27, 872–887. doi:10.1007/s12613-019-1956-9

Moore, T. A. (2012). Coalbed methane: a review. *Int. J. Coal Geol.* 101, 36–81. doi:10.1016/j.coal.2012.05.011

Niu, Q. H., Pan, J. N., Jin, Y., Wang, H. C., Li, M., Ji, Z. M., et al. (2019). Fractal study of adsorption-pores in pulverized coals with various metamorphism degrees using $N_2$ adsorption, X-ray scattering and image analysis methods. *J. Pet. Sci. Eng.* 176, 584–593. doi:10.1016/j.petrol.2019.01.107

Pan, J. N., Lv, M. M., Hou, Q. L., Han, Y. Z., and Wang, K. (2019). Coal microcrystalline structural changes related to methane adsorption/desorption. *Fuel* 239 (1), 13–23. doi:10.1016/j.fuel.2018.10.155

Qin, Y., Moore, T. A., Shen, J., Yang, Z. B., Shen, Y. L., and Wang, G. (2018). Resources and geology of coalbed methane in China: a review. *Int. Geol. Rev.* 60 (5-6), 777–812. doi:10.1080/00206814.2017.1408034

Shen, W. L., Shi, G. C., Wang, Y. G., Bai, J. B., Zhang, R. F., and Wang, X. Y. (2021). Tomography of the dynamic stress coefficient for stress wave prediction in sedimentary rock layer under the mining additional stress. *Int. J. Min. Sci. Technol.* 31, 653–663. doi:10.1016/j.ijmst.2021.04.003

Sinha, S. K., and Gupta, S. D. (2021). A geological model for enhanced coal bed methane (ECBM) recovery process: A case study from the jharia coalfield region, India. *J. Pet. Sci. Eng.* 201, 108498. doi:10.1016/j.petrol.2021.108498

Su, Y. F. (2016). Three gases Co-exploration and Co-mining of sea-land transition phase coal measures in Shanxi province, CNKI:SUN:ZGMC.0.2016-06-002. *China Coalbed Methane* 13 (6), 8–11. (in Chinese with English abstract).

Wang, K., and Du, F. (2020). Coal-gas compound dynamic disasters in China: a review. *Process Saf. Environ. Prot.* 133, 1–17. doi:10.1016/j.psep.2019.10.006

Wang, C., Xiong, Z. Q., Wang, C., Wang, Y. L., and Zhang, Y. H. (2020). Study on rib sloughage prevention based on geological structure exploration and deep borehole grouting in front abutment zones. *Geofluids* 2020, 1–12. doi:10.1155/2020/7961032

Wang, Z. Q., Yan, E. C., and Ji, H. B. (2016). *In-situ* stress field and geological tectonic analysis at Huangdao water-sealed underground oil carven site. *J. Eng. Geol.* 24 (1), 136–141. (in Chinese with English abstract). doi:10.13544/j.cnki.jeg.2016.01.017

Wang, C., Song, D. Z., Zhang, C. L., Liu, L., Zhou, Z. H., and Huang, X. C. (2019). Research on the classification model of coal's bursting liability based on database with large samples. *Arab. J. Geosci.* 12 (13), 411. doi:10.1007/s12517-019-4562-2

Wang, K., Yang, P., Yu, G. M., Yang, C., and Zhu, L. Y. (2020). 3D numerical modelling of tailings dam breach run out flow over complex terrain: A multidisciplinary procedure. *Water* 12 (9), 2538. doi:10.3390/w12092538

Xie, W. D., Wang, M., and Hou, X. W. (2018). Study on enrichment zones and enrichment regularity of coalbed methane in Hebei province. *J. Henan Polytech. Univ. Nat. Sci.* , 37 (182), 22–30. (in Chinese with English abstract). doi:10.16186/j.cnki.1673-9787.2018.03.003

Ye, Z. N., Hou, E. K., Duan, Z. H., and Li, Z. J. (2019). Coal reservoir characterization in a tectonic setting and the effects of tectonism on the coalbed methane (CBM) content. *Adv. Mater. Sci. Eng.* 2019, 1–11. doi:10.1155/2019/7974628

Yu, S. J., Liu, J. Y., Bai, P., Xu, H. T., He, R. S., Wang, Y. S., et al. (2021). Geological structure exploration of karst collapse column and evaluation of water insulation properties of the mud part. *Geofluids* 2021, 1–9. doi:10.1155/2021/2071333

Yuan, B. X., Li, Z. H., Chen, Y. M., Ni, H., Zhao, Z. Q., Chen, W. J., et al. (2021). Mechanical and microstructural properties of recycling granite residual soil reinforced with glass fiber and liquid-modified polyvinyl alcohol polymer. *Chemosphere* 268, 131652. doi:10.1016/j.chemosphere.2021.131652

Zhang, C. L., Wang, E. Y., Xu, J., and Peng, S. J. (2020). Research on temperature variation during coal and gas outbursts: Implications for outburst prediction in coal mines. *Sensors* 20 (19), 5526. doi:10.3390/s20195526

Zhang, C. L., Wang, E. Y., Xu, J., and Peng, S. J. (2021). A new method for coal and gas outburst prediction and prevention based on the fragmentation of ejected coal. *Fuel* 287, 119493. doi:10.1016/j.fuel.2020.119493

Zhang, X. M., Li, J. W., Han, B. S., and Dong, M. T. (2005). Division and formation mechanism of coalbed methane reservoir in Huainan Coalfield, Anhui Province, China. *Chin. Sci. Bull.* 50 (S), 7–17. doi:10.1007/BF03184077

Zhang, Z. B., Liu, X. N., Zhang, Y. H., Qin, X. Y., and Khan, M. (2021a). Comparative study on fracture characteristics of coal and rock samples based on acoustic emission technology. *Theor. Appl. Fract. Mech.* 111, 102851. doi:10.1016/j.tafmec.2020.102851

Zhang, Z. B., Wang, E. Y., Liu, X. N., Zhang, Y. H., Li, S. J., Khan, M., et al. (2021b). Anisotropic characteristics of ultrasonic transmission velocities and stress inversion during uniaxial compression process. *J. Appl. Geophy.* 186, 104274. doi:10.1016/j.jappgeo.2021.104274

Zhang, K. Z., Wang, L., Cheng, Y. P., Li, W., Kan, J., Tu, Q. Y., et al. (2020). Geological control of fold structure on gas occurrence and its implication for coalbed gas outburst: Case study in the Qinan coal mine Huaibei Coalfield, China. *Nat. Resour. Res.* 29, 1375–1395. doi:10.1007/s11053-019-09511-7

Zhang, R., Liu, J., Sa, Z. Y., Wang, Z. Q., Lu, S. Q., and Lv, Z. Y. (2020). Fractal characteristics of acoustic emission of gas-bearing coal subjected to true triaxial loading. *Measurement* 169, 108349. doi:10.1016/j.measurement.2020.108349

Zheng, C. S., Jiang, B. Y., Xue, S., Chen, Z. W., and Li, H. (2019). Coalbed methane emissions and drainage methods in underground mining for mining safety and environmental benefits: A review. *Process Saf. Environ. Prot.* 127, 103–124. doi:10.1016/j.psep.2019.05.010

Zhou, Y. B., Li, Z. H., Zhang, R. L., Wang, G. Z., Yu, H., Sun, G. Z., et al. (2019). $CO_2$ injection in coal: Advantages and influences of temperature and pressure. *Fuel* 236 (1), 493–500. doi:10.1016/j.fuel.2018.09.016

Zhou, Y. B., Li, H. S., Huang, J. L., Zhang, R. L., Wang, S. J., Hong, Y. D., et al. (2021). Influence of coal deformation on the Knudsen number of gas flow in coal seams. *Energy* 233, 121161. doi:10.1016/j.energy.2021.121161

Zhou, X. M., Wang, S., Li, X. L., Meng, J., Li, Z., Zhang, L., et al. (2022). Research on theory and technology of floor heave control in semicoal rock roadway: Taking longhu coal mine in Qitaihe mining area as an Example. *Lithosphere* 2022 (11), 3810988. doi:10.2113/2022/3810988

Zou, M. J., Wei, C. T., Huang, Z. Q., and Wei, S. (2015). Porosity type analysis and permeability model for micro-trans-pores, meso-macro-pores and cleats of coal samples. *J. Nat. Gas. Sci. Eng.* 27, 776–784. doi:10.1016/j.jngse.2015.09.025

Zou, M. J., Wei, S. M., Huang, Z. Q., Lv, X., and Guo, B. (2018). Simulations on recoverability performances for a coalbed methane field in SE edge of Ordos basin, China. *Fuel* 233, 354–360. doi:10.1016/j.fuel.2018.06.071

Zou, M. J., Wei, C. T., Zhang, M., and Lv, X. (2018). Quantification of gas and water transfer between coal matrix and cleat network during drainage process. *J. Energy Resour. Technol.* 140, 032905–032919. doi:10.1115/1.4038044

Zou, M. J., Lv, X. C., Huang, Z. Q., Wei, S., Zhang, M., and Sun, C. (2018). Modeling and prediction for gas production during coalbed methane drainage based on two indirect reservoir parameters. *Energy Explor. Exploit.* 36 (6), 1424–1437. doi:10.1177/0144598718777105

Zou, M. J., Liu, Y. Z., Huang, Z. Q., Zhang, M., and Zhang, P. (2020). Geological control of irreducible water within the coal matrix and its quantified evaluation model. *ACS Omega* 5, 9540–9549. doi:10.1021/acsomega.0c00782

Zou, Q. L., Liu, H., Zhang, Y. J., Li, Q. M., Fu, J. W., and Hu, Q. T. (2020). Rationality evaluation of production deployment of outburst-prone coal mines: A case study of nantong coal mine in chongqing, China. *Saf. Sci.* 122, 104515. doi:10.1016/j.ssci.2019.104515